Digest Journal of Nanomaterials and Biostructures Vol. 8, No. 4, October – December 2013, p. 1591 - 1600

MORPHOLOGY-CONTROLLED SYNTHESIS OF ZnO STRUCTURES BY A SIMPLE WET CHEMICAL METHOD

N. PREDA*, M. ENCULESCU, C. FLORICA, A. COSTAS,
A. EVANGHELIDIS, E. MATEI, I. ENCULESCU
National Institute of Materials Physics, Multifunctional Materials and Structures Laboratory, Bucharest, P.O. Box MG-7, R-77125, Romania

Zinc oxide particles were synthesized by a simple wet chemical method. Using zinc nitrate and various precipitating agents, like KOH, NaOH and $(CH_2)_6N_4$, particles with different morphologies were obtained. Also, the addition of a structure-directing agent, like gum arabic - a highly branched biopolymer, leads to a decrease in the ZnO particles size (for KOH and NaOH) and to a dramatical change of the ZnO particle shape in the case of $(CH_2)_6N_4$. The X-ray diffraction analysis showed that all obtained samples are of wurtzite structure. The reflectance and photoluminescence spectra have been used to investigate the optical properties of the ZnO structures. The morphologies observed by scanning electron microscopy reveal snowflake-like, flower-like, star-like and double-raspberry-like structures. A possible formation mechanism for ZnO micro/nanostructures with different morphologies was proposed. The biopolymer-assisted crystallization method could provide a facile approach to synthesize other desired compounds with controllable morphology.

(Received October 5, 2013; Accepted November 8, 2013)

Keywords: ZnO micro/nanostructures; wet chemical method; gum arabic; scanning electron microscopy

1. Introduction

One of the most attracting semiconductor materials is zinc oxide due to its properties (direct band gap, large exciton binding energy, strong luminescence, high thermal conductivity, etc.) and for its potential in diverse technologically fields (optics, optoelectronics, catalysis, piezoelectricity, solar cells, superhydrophobic surfaces, biosensors, etc.) [1-5]. A considerable effort has been made in the last years for controlling the morphology of ZnO low-dimensional particles in order to tune their properties, these being significantly influenced by the particles shape, size, size distribution and aspect ratio (width-to-length ratio). There are lots of ways for synthesis of ZnO micro-and nano-structures, this compound possessing a rich family of structures such as whiskers, wires, rods, tubes, belts, cages, rings, combs, prisms, etc. [5-12]. All these morphologies featured by properties for different applications lead to the development of research on the synthesis of ZnO by various methods [13-16]: physical (chemical vapor deposition, molecular beam epitaxy, pulsed laser deposition, magnetron sputtering, thermal evaporation) and chemical (chemical bath deposition, electrochemical deposition, hydrothermal, solvothermal, sol-gel). The physical methods have some disadvantages: the techniques are time-consuming, the used equipments are expensive, the reaction temperature is high, etc. On the other hand, the chemical methods showed the following advantages: relatively low temperature (below 100 ^{0}C), use of inexpensive equipment, large area deposition and low cost, which is more attractive for mass production. Among the chemical methods, the precipitation reaction is a relatively simple wet chemical technique which can produce micro- and nano-particles with different morphologies and

*Corresponding author: nicol@infim.ro

better crystalline quality. Additionally, when a structure-directing agent like surfactants [17, 18] or polymers [19-21] is added in the water during the ZnO particles synthesis, this can change dramatically the morphology and size of the semiconductor particles. From the polymers, the biopolymers like polysaccharides (PSH) have attracted recently much attention in the research regarding the synthesis of ZnO crystallites [22-30]. PSH, such as gelatin [25, 26], starch [27, 28] or gum arabic [29, 30] are particularly interesting since their chains contain a high number of functional groups that are able to coordinate with the metal ions leading to a homogeneous dispersion of the cations in the PSH. When a precipitation agent is added, the metal-occupied positions become incipient sites of nucleation and initial growth of crystallites which lately will aggregate and finally form the semiconducting particles. In the case of highly branched PSH, due to the numerous interior cavities, as well as inward and outward oriented functional groups, the semiconductor crystallites growth can takes place in the free space with a direct consequence on the uniform particles size.

In this context, the present work is focused on the influence of precipitating agents such as KOH, NaOH and $(CH_2)_6N_4$ on formation of different ZnO morphologies. Another goal of this study is the effect of gum arabic, a highly branched biopolymer added during the precipitation reaction, on the shape and size of ZnO particles. The morphological, structural and optical properties of the ZnO crystallites were studied using scanning electron microscopy, X-ray diffraction, optical spectroscopy and photoluminescence. We note that, to our knowledge, only two papers [29, 30] were published about the gum arabic-assisted aqueous synthesis of ZnO particles with hexagonal prims [29] or twin-brush [30] shape. In both cases, the studies followed only the influence of reaction parameters (time reaction, temperature reaction, reactants nature, the way the reactant solutions are mixed, etc.) on the nucleation and growth of the ZnO crystallites.

2. Experimental

The ZnO crystallites were prepared by the chemical reaction between zinc nitrate and different precipitating agents: potassium hydroxide (KOH), sodium hydroxide (NaOH) and hexamethylenetetramine ($(CH_2)_6N_4$). All reactants, inclusive gum arabic (GA) were purchased from Sigma-Aldrich.

In the first step, 0.01 M $Zn(NO_3)_2$ aqueous solution was prepared. This solution was placed in thermostatic bath under continuous stirring and a 0.01 M precipitating agent water solution was added when it reached 90 ^{0}C. The appearance of the white color is the first evidence of the formation of ZnO crystallites. After 3 h the white powder was collected through centrifugation, washed several times with distilled water and dried on filter paper at room temperature.

Next we evaluated the influence of GA on the ZnO morphology. Maintaining all the other reaction parameters constant we synthesized ZnO particles using 0.01 % concentration of GA. The as-prepared powders were separated by centrifugation. Then the precipitates were washed with distilled water and centrifuged several times in order to dissolve the GA. Finally, the white powders were dried in air at room temperature.

The crystalline phase of the powder samples was identified by X-ray diffraction (XRD) on a Bruker AXS D8 Advance instrument with Cu Kα radiation (λ = 0.154 nm). The source was operated at 40 kV and 40 mA and the Kβ radiation was eliminated using a nickel filter. The optical properties of the ZnO powders were investigated by measuring the reflection spectra using a Perkin-Elmer Lambda 45 UV-VIS spectrophotometer equipped with an integrating sphere. The photoluminescence (PL) measurements were performed at 350 nm excitation wavelength using FL 920 Edinburgh Instruments spectrometer with a 450 W Xe lamp excitation and double monochromators on both excitation and emission. All PL spectra were recorded in the same experimental conditions (excitation wavelength = 350 nm, step, dwell time, slits). The morphologies of the powder samples were evaluated using a Zeiss Evo 50 XVP scanning electron microscope (SEM). The samples were sputtered with a thin layer of gold prior to imaging.

3. Results and discussion

The structure of the samples was examined by X-ray diffraction. The diffractograms from Fig. 1 show main peaks at 2θ: 31.8^0; 34.5^0, 36.3^0, 47.5^0, 56.6^0, 63.0^0, 66.4^0, 68.0^0 and 69.1^0 which correspond to the Miller index of the reflecting planes for (100), (002), (101), (102), (110), (103), (200), (112) and (201). All the observed diffraction peaks are assigned to ZnO hexagonal wurtzite phase (JCPDS file no. 36-1451), and confirm the formation of ZnO crystallites. The strong and sharp diffraction peaks suggest that the as-obtained products are well crystallized. In the XRD patterns of all samples no peaks characteristic to any segregate phases, such as $Zn(OH)_2$, were observed. It has to be noticed that for the ZnO samples synthesized in the presence of GA (curves b, d and f), the widths of diffraction peaks are larger than those observed for the ZnO crystallites synthesized in the absence of biopolymer (curves a, c and e) suggesting that the particle size becomes slightly smaller. Also, it is worth noting that compared to the standard file of ZnO hexagonal wurtzite, the relative intensity of (100) peak is much stronger than the one of (002) peak when $(CH_2)_6N_4$ was used as precipitating agent (curve e) which may be attributed to a preferential direction growth of ZnO crystallites.

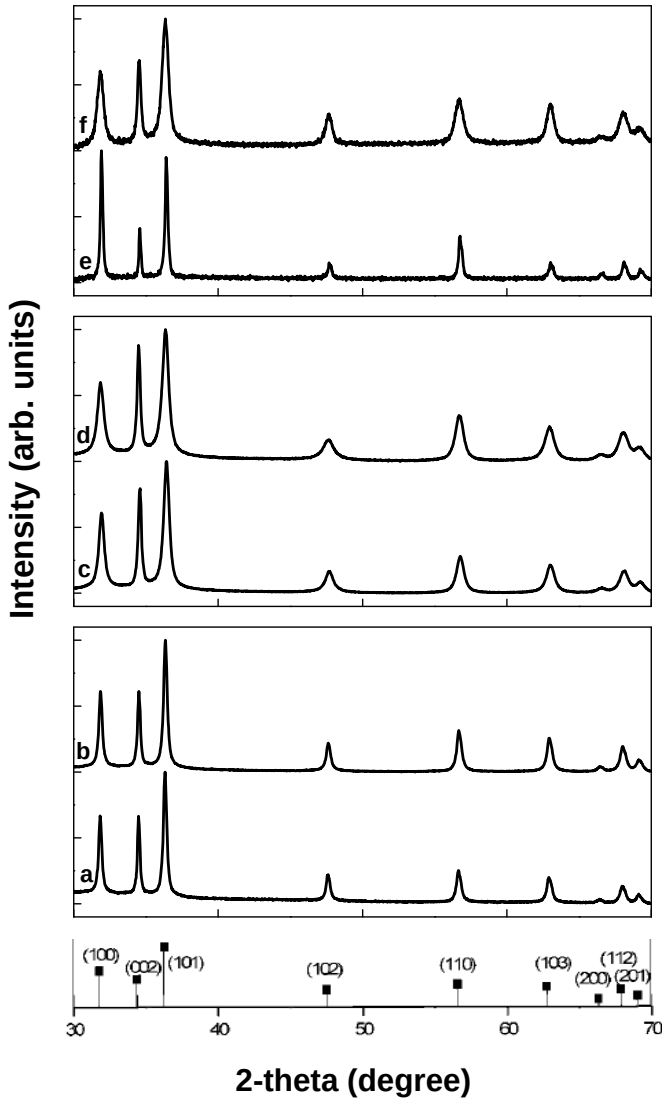

Fig. 1. Powder XRD patterns of ZnO crystallites prepared from $Zn(NO_3)_2$ and KOH, NaOH, $(CH_2)_6N_4$ in the absence of GA (a, c, e) and in the presence of GA: (b, d, f).

The changes in the optical properties of ZnO crystallites synthesized in the presence of different precipitating agents and structure-directing agent are observed in Fig. 2. In the all spectra of the ZnO structures, a strong decrease of reflectance can be noticed below 400 nm, this being linked to the band-to-band transition in ZnO. Based on the reflectance data, the band gap of all samples is estimated by plotting $[F(R)\cdot E]^2$ versus photon energy (E), where F(R) is the Kubelka-Munk function with $F(R) = (1-R)^{1/2} / 2R$ and R is the observed diffuse reflectance. From the Kubelka-Munk representation (inset Fig. 2) the band gap values are about: i) 3.30 eV (curve a), 3.27 eV (curve c) and 3.28 eV (curve e) in the absence of GA and ii) 3.32 eV (curve b), 3.33 eV (curve d) and 3.31 eV (curve f) in the presence of GA, in agreement with those reported for ZnO in the literature.

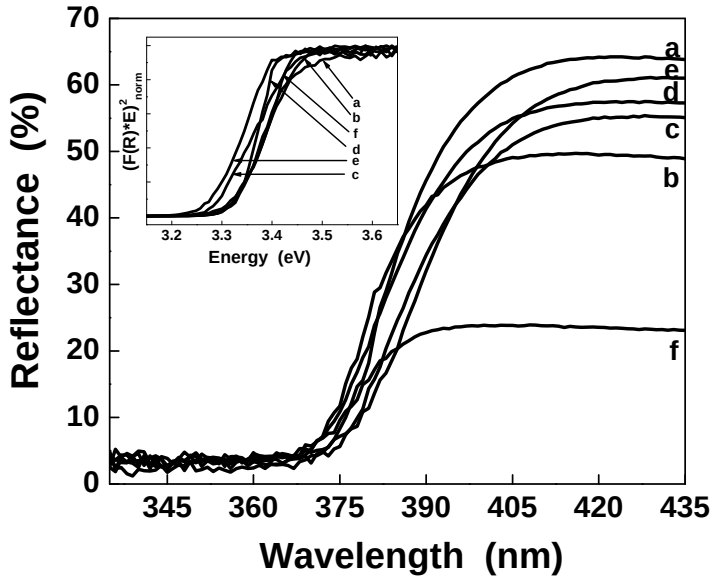

Fig. 2. Reflectance spectra of ZnO crystallites prepared from $Zn(NO_3)_2$ and KOH, NaOH, $(CH_2)_6N_4$ in the absence of GA (a, c, e) and in the presence of GA: (b, d, f).

In the inset is shown the normalized representation of Kubelka-Munk function employed to estimate the band gap values of ZnO crystallites.

The emission spectra of ZnO samples are presented in Fig. 3. Typically in the PL spectra of ZnO there are emission bands in the UV and visible regions [31]. In our case, the PL spectra of synthesized ZnO samples display two PL emissions: an UV emission centered at ~3.27 eV (curve e – without GA and curve f – with GA) and a green emission at ~2.20 eV (observed in the all PL spectra). The UV emission has an excitonic origin and the other emission band originates from defect emission. Although the mechanism of the visible emission in ZnO crystals has not been conclusively established, models related to various defects which can provide recombinations centers within the band gap, have been proposed and reviewed in Ref. [32]. This emission is usually attributed to the oxygen vacancies and the incorporation of hydroxyl groups in the crystal lattice during solution growth [33, 34]. In our opinion, the high intensity of the visible emission is linked to the increase of the defect density in the ZnO structures synthesized by this wet chemical method [35].

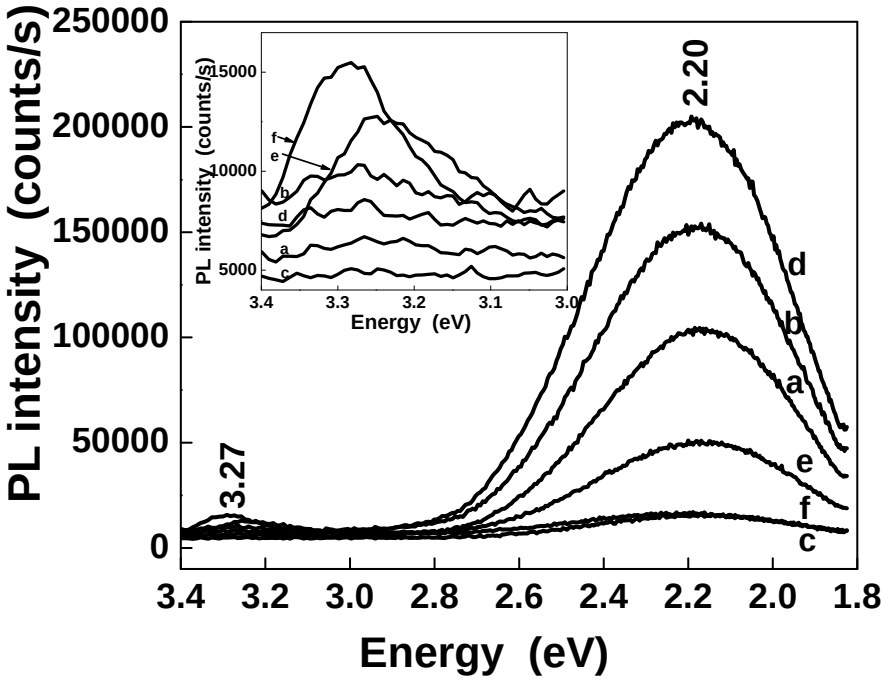

Fig. 3. Photoluminescence spectra of ZnO crystallites prepared from $Zn(NO_3)_2$ and KOH, NaOH, $(CH_2)_6N_4$ in the absence of GA (a, c, e) and in the presence of GA: (b, d, f). In the inset is shown only the higher energy region.

The next step was to investigate by SEM technique the morphologies of all samples (Fig. 4). In the absence of GA, particles like snow-flakes (Fig. 4a), flowers (Fig. 4c) and stars (Fig. 4e) with sizes in the range of 1-3 μm were synthesized. The influence of the GA on the shape of the ZnO crystallites is observed in Fig. 4a, 4d and 4f. Thus, the particles shape did not alter when GA was added into the KOH or NaOH solutions (Fig. 4b and Fig. 4d, respectively), only their size decreasing at about 500 nm-1.5 μm. In contrast, the morphology is dramatically changed when GA was added into $(CH_2)_6N_4$ solution. The stars-like structures became double-raspberry-like structures with a relatively uniform size in the range of 200-400 nm (Fig. 4f). More informations regarding the ZnO structures morphology were obtained from the higher magnification SEM images (Fig. 5). As it can be seen in all cases ZnO particles are self-assembled in complex agglomerated structures: the snow-flakes contain platelets (Fig. 5a and Fig. 5b), the flowers have many (Fig. 5c) or few petals (Fig. 5d), the stars are formed by hexagonal prismatic rods (Fig. 5e) and the double-raspberries are also particles aggregated into organized structures (Fig. 5f).

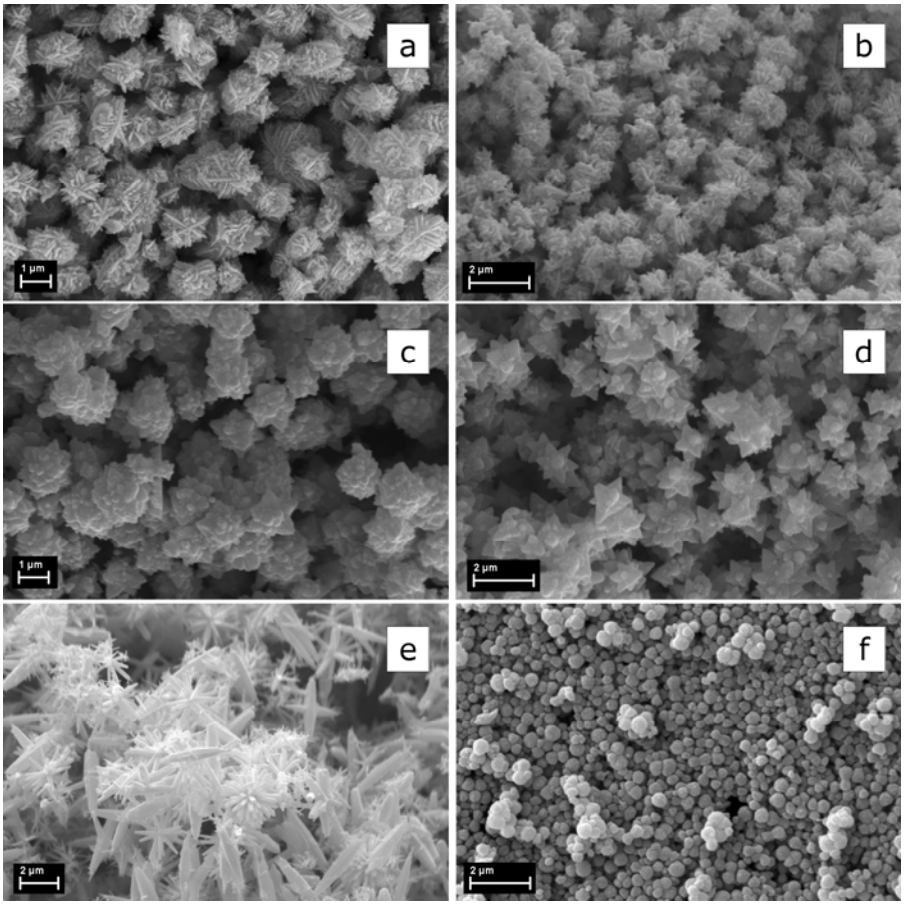

Fig. 4. SEM images of of ZnO crystallites prepared from $Zn(NO_3)_2$ and KOH, NaOH, $(CH_2)_6N_4$ in the absence of GA (a, c, e) and in the presence of GA: (b, d, f).

Generally, the synthesis of colloid crystallites includes two processes: nucleation and growth. For specific growth conditions, the nucleation and the growth rates of different crystal facets determine the overall structure and morphology. In order to explain how different precipitating agents influence the ZnO morphology, in the following are described the possible reactions involved in the ZnO synthesis, according with Ref. [36]:

i) using strong base (KOH, NaOH)

$Zn(NO_3)_2 \rightarrow Zn^{2+} + 2NO_3^-$ (a)

$Zn^{2+} + 2HO^- \rightarrow Zn(OH)_2$ (b)

$Zn(OH)_2 + 2HO^- \rightarrow [Zn(OH)_4]^{2-}$ (c)

$[Zn(OH)_4]^{2-} \rightarrow ZnO \downarrow + 2HO^- + H_2O$ (d)

ii) using weak base ($(CH_2)_6N_4$)

$Zn(NO_3)_2 \rightarrow Zn^{2+} + 2NO_3^-$ (a)

$(CH_2)_6N_4 + 6H_2O \rightarrow 6HCHO + 4NH_3$ (b)

$NH_3 + H_2O \rightarrow NH_4^+ + HO^-$ (c)

$Zn^{2+} + 3NH_4^+ \rightarrow [Zn(NH_3)_4]^{2+}$ (d)

$[Zn(NH_3)_4]^{2+} + 2HO^- \rightarrow Zn(OH)_2 + 4NH_3$ (e)

$Zn(OH)_2 \rightarrow ZnO \downarrow + H_2O$ (f)

Initially, in the strong alkaline aqueous solutions, $Zn(NO_3)_2$ and the base (KOH or NaOH) undergo hydrolysis and produce Zn^{2+} ions and HO^- ions, which latter produce $Zn(OH)_2$. Because of the alkali excess, $Zn(OH)_2$ react further with HO^- to form $[Zn(OH)_4]^{2-}$ complexes. The heating causes the decomposition of these species to ZnO nuclei. Successively growth and aggregation

processes lead to the appearance of ZnO crystallites and finally to the ZnO complex structures formation. The different $[Zn(OH)_4]^{2-}$ precursors can modify the reaction process, which may affect the competition between thermodynamics and kinetics during the reduction of precursors, nucleation and growth of ZnO crystals. The formation of different structures in the alkali solutions (snow-flakes or flowers) depends greatly on the nucleation frequency of ZnO. Being the predominant ions in the solution, hydroxyl ions play a crucial role in controlling the synthesis of the different crystalline facets because of the greater formation of $[Zn(OH)_4]^{2-}$ complexes. Negatively charged, these species will preferably adsorb on the surface of ZnO nuclei positively charged.

In the case of $(CH_2)_6N_4$, its exact function in the ZnO synthesis is still unclear. Non-ionic cyclic tertiary amine, it can act as a bidentate Lewis ligand capable of bridging two Zn^{2+} ions in solution [37]. Moreover, it has been suggested [38] that it is preferentially attached to the non-polar facets of the ZnO crystallite cutting off the access of zinc ions to them and leaving only the polar (001) face for growth. $(CH_2)_6N_4$ is also known as weak base and pH buffer [39]. So, when $(CH_2)_6N_4$ is used, in the first step, by its thermal decomposition ammonia and formaldehyde were produced. Zinc ions resulted from the zinc nitrate hydrolysis form with ammonia $[Zn(NH_3)_4]^{2+}$ complexes. At higher temperature these complexes decompose leading to the release of Zn^{2+} and HO^- ions into solution, these form the $Zn(OH)_2$ which is thermal dehydrated to ZnO.

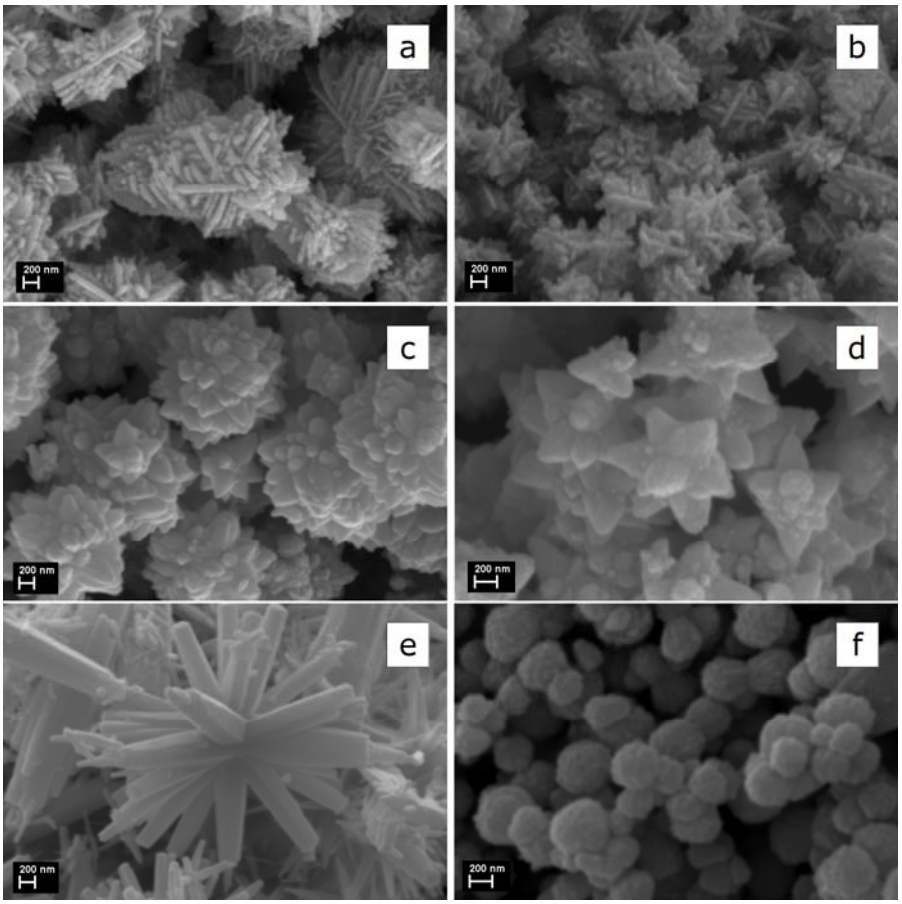

Fig. 5. Higher magnification SEM images of of ZnO crystallites prepared from $Zn(NO_3)_2$ and KOH, NaOH, $(CH_2)_6N_4$ in the absence of GA (a, c, e) and in the presence of GA: (b, d, f).

The presence of GA during the ZnO synthesis can affect less or more the ZnO mechanism formation, depending on the precipitating agent used as reactant. From the SEM images, it can be observed that GA affects only slightly the particles shape in the case of strong alkaline agents (KOH and NaOH), when HO^- ions are release very fast in the aqueous solutions (both the

nucleation and growth steps were fast) and change dramatically the particles shape when a weak base like $(CH_2)_6N_4$ is used as steady source for slowly release of HO^- ions. In the last case, the homogeneous release of hydroxyl ions correlated with the presence of GA can lead to the formation of uniform size ZnO structures like double-raspberry structures. As highly branched polysaccharide, GA presents numerous interior cavities, so the ZnO growth can take place in the free space due to these cavities having as consequence a limiting size effect on ZnO particles (Scheme 1). But, as polysaccharide, GA can form also complexes with Zn^{2+} ions [24] because of its high number of inward and outward oriented reactive functional groups (-COOH, -OH and -NH_2) (Scheme 1). Therefore, the zinc ions are closely associated with the GA chains, in this way the zinc-occupied sites can become incipient centers of nucleation and initial growth of crystallites which further aggregate and finally form the ZnO particles. The whole formation mechanism and the growth of ZnO crystallites in the presence of a hyperbranched biopolymer are to complex to give an exact explanation, but the possible reactions implied in the ZnO synthesis using GA can be the following:

i) using strong base (KOH, NaOH)

$$Zn(NO_3)_2 \rightarrow Zn^{2+} + 2NO_3^- \quad (a)$$

$$yZn^{2+} + GA \rightarrow [Zn(GA)]^{2y+} \quad (b)$$

$$[Zn(GA)]^{2y+} + 2yHO^- \rightarrow \{[yZn(OH)_2]GA\} \quad (c)$$

$$\{[yZn(OH)_2]GA\} + 2yHO^- \rightarrow \{\{[Zn(OH)_4]^{2y-}\}GA\} \quad (d)$$

$$\{\{[Zn(OH)_4]^{2y-}\}GA\} \rightarrow [(yZnO)GA]\downarrow + 2yHO^- + yH_2O \quad (e)$$

ii) using weak base ($(CH_2)_6N_4$)

$$Zn(NO_3)_2 \rightarrow Zn^{2+} + 2NO_3^- \quad (a)$$

$$yZn^{2+} + GA \rightarrow [Zn(GA)]^{2y+} \quad (b)$$

$$(CH_2)_6N_4 + 6H_2O \rightarrow 6HCHO + 4NH_3 \quad (c)$$

$$NH_3 + H_2O \rightarrow NH_4^+ + HO^- \quad (d)$$

$$[Zn(GA)]^{2y+} + + 2yHO^- \rightarrow \{[yZn(OH)_2]GA\} \quad (e)$$

$$\{[yZn(OH)_2]GA\} \rightarrow [(yZnO)GA]\downarrow + yH_2O \quad (f)$$

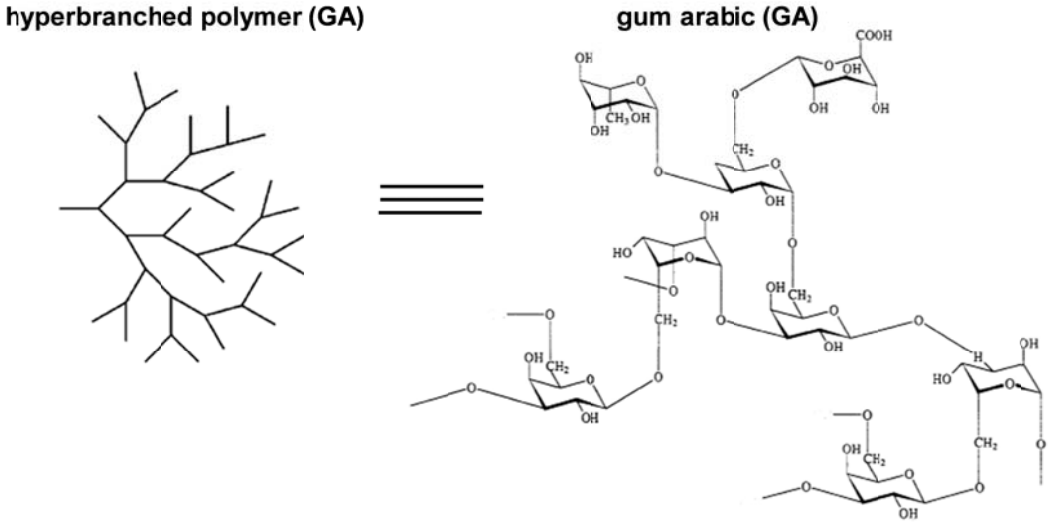

Scheme 1. Gum arabic structure

These results conclude that both the precipitating agent and the biopolymer significantly control the crystal growth of ZnO structures and in this way their morphology.

4. Conclusions

By a simple wet chemical method, using different precipitating agents KOH, NaOH and $(CH_2)_6N_4$) and a structure-directing agent (gum arabic) we obtain ZnO structures with complex morphology such as snow-flake, flower, star, and double-raspberry. The sharp and intense XRD diffraction peaks prove that the ZnO particles are well crystallized in wurtzite structure. The reflectance and photoluminescence spectra have been used to investigate the optical properties of the ZnO structures. A possible formation mechanism for ZnO micro/nanostructures was proposed. It is expected that the information about how to manipulate the ZnO morphology using gum arabic can be easily extended to similar oxide semiconductor particles and other polysaccharides. The simplicity and cheapness of the technique which does not require complex apparatus and the availability of raw reagents are advantages favoring the scaling-up of the method.

Acknowledgements

This work was supported by a grant of the Romanian National Authority for Scientific Research, CNCS – UEFISCDI, project number PN-II-RU-TE-2012-3-0148.

References

[1] Z. L. Wang, X. Y. Kong, Y. Ding, P. Gao, W. L. Hughes, R. Yang, Y. Zhang, Adv. Funct. Mater. **14**, 943 (2004)
[2] A. Janotti, C. G. Van de Walle, Rep. Prog. Phys. **72**, 126501 (2009)
[3] M. Ahmad, J. Zhu, J. Mater. Chem. **21**, 599 (2011)
[4] Z. L. Wang, MRS Bulletin, **37**, 814 (2012)
[5] N. Preda, M. Enculescu, I. Zgura, M. Socol, E. Matei, V. Vasilache, I. Enculescu, Mater. Chem. Phys., **138**, 253 (2013)
[6] Z. L. Wang, Mater. Sci. Eng. R **64**, 33 (2009)
[7] A. B. Djurisic, X. Chen, Y. H. Leung, A. M. C. Nq, J. Mater. Chem. **22**, 6526 (2012)
[8] S. K. Arya, S. Saba, J. E. Ramirez-Vick, V. Gupta, S. Bhansali, S. P. Singh, Anal. Chim. Acta **737**, 1 (2012)
[9] L. Loh, S. Dunn, J. Nanosci. Nanotechnol. **12**, 8215 (2012)
[10] S. Sun, X. Zhang, J. Zhang, X. Song, Z. Yang, Cryst. Growth Des., **12**, 2411 (2012)
[11] Y. Zhang, X. Yan, Y. Yang, Y. Huang, Q. Liao, J. Qi, Adv. Mater. **24**, 4647 (2012)
[12] N. Preda, M. Enculescu, I. Enculescu, Soft Mater **11**, 457 (2013)
[13] D. P. Singh, Sci. Adv. Mater., **2**, 245 (2010)
[14] G. Jia, Y. Wang, J. Yao, Digest J. Nanomater. Bios., **7**, 261 (2012)
[15] P. K. Baviskar, P. R. Nikam, S. S. Gargote, A. Ennaoui, B. R. Sankapal, J. Alloys Compd. **551**, 233 (2013)
[16] M. Sui, P. Gong, X. Gu, Front. Optoelectron., on line article, DOI 10.1007/s12200-013-0357-3 (2013)
[17] N. Samaele, P. Amornpitoksuk, S. Suwanboon, Powder Technol. **203**, 243 (2010)
[18] D. Geetha, T. Thilagavathi, Digest J. Nanomater. Bios., **5**, 297 (2010)
[19] Y. Peng, A.-W. Xu, B. Deng, M. Antonietti, H. Colfen, J. Phys. Chem. B, **110**, 2988 (2006)
[20] D. Zhang, G. Zhang, Y. Liao, C. Wang, Y. Chen, H. Lin, H. Morikawa, Mater. Lett. **102**-103, 98 (2013)
[21] M. K. Debanath, S. Karmakar, Mater. Lett., 111, 116 (2013)
[22] S. Gao, H. Zhang, X. Wang, R. Deng, D. Sun, G. Zheng, J. Phys. Chem. B, **110**, 15847 (2006)
[23] M. M. Tomczak, M. K. Gupta, L. F. Drummy, S. M. Rozenzhak, R. R. Naik, Acta Biomater., **5**, 876 (2009)
[24] M. Thirumavalavan, K. L. Huang, J. F. Lee, Colloids Surf. A: Physicochem. Eng. Aspects, **417**, 154 (2013)

[25] Y.-H. Tseng, H.-Y. Lin, M.-H. Liu, Y.-F. Chen, C.-Y. Mou, J. Phys. Chem. C, **113**, 18053 (2009)
[26] Y.-H. Tseng, M.-H. Liu, Y.-W. Kuo, P. Chen, C.-T. Chen, Y.-F. Chen, C.-Y. Mou, Chem. Commun., **48**, 3215 (2012)
[27] P. Mishra, R. S. Yadav, A. C. Pandey, Digest J. Nanomater. Bios., **4**, 193 (2009)
[28] G. Zhang, X. Shen, Y. Yang, J. Phys. Chem. C, **115**, 7145 (2011)
[29] M. Jitianu, D. V. Goia, J. Colloid. Interf. Sci., **309**, 78 (2007)
[30] M.-H. Liu, Y.-H. Tseng, H. F. Greer, W. Zhou, C.-Y. Mou, Chem. Eur. J., **18**, 16104 (2012)
[31] A. B. Djurisic, A. M. C. Ng, X. Y. Chen, Progress Quant. Electron., **34**, 191 (2010)
[32] A. B. Djurisic, Y. H. Leung, Small, **2**, 944 (2006)
[33] K. H. Tam, C. K. Cheung, Y. H. Leung, A. B. Djurisic, C. C. Ling, C. D. Beling, S. Fung, W. M. Kwok, W. K. Chan, D. L. Phillips, L. Ding, W. K. Ge , J. Phys. Chem. B, **110**, 20865 (2006)
[34] D. Li, Y. H. Leung, A. B. Djurisic, Z. T. Liu, M. H. Xie, S. L. Shi, S. J. Xu, W. K. Chan, Appl. Phys. Lett., **85**, 1601 (2004)
[35] C. H. Hung, W. T. Whang, J. Mater. Chem., **15**, 267 (2005)
[36] S. Xu, Z. L. Wang, Nano Res., **4**, 1013 (2011)
[37] I. S. Ahuja, C. L. Yadava, R. Singh, J. Mol. Struct., **81**, 229 (1982)
[38] A. Sugunan, H. C. Warad, M. Boman, J. Dutta, J. Sol-Gel Sci. Techn., **39**, 49 (2006)
[39] K. Govender, D. S. Boyle, P. B. Kenway, P. O'Brien, J. Mater. Chem., **14**, 2575 (2004)